120-GHz-Band Wireless Link Technologies for Outdoor 10-Gbit/s Data Transmission

Akihiko Hirata, *Senior Member, IEEE*, Toshihiko Kosugi, Hiroyuki Takahashi, *Member, IEEE*, Jun Takeuchi, Hiroyoshi Togo, *Senior Member, IEEE*, Makoto Yaita, Naoya Kukutsu, *Member, IEEE*, Kimihisa Aihara, *Member, IEEE*, Koichi Murata, *Senior Member, IEEE*, Yasuhiro Sato, *Member, IEEE*, Tadao Nagatsuma, *Senior Member, IEEE*, and Yuichi Kado, *Member, IEEE*

***Abstract*—Our progress in 120-GHz-band wireless link technologies enables us to transmit 10-Gbit/s data transmission over a distance of more than 1 km. The 120-GHz-band wireless link uses high-speed uni-traveling carrier photodiodes (UTC-PD) and InP high-electron mobility transistor (HEMT) millimeter-wave (MMW) monolithic integrated circuits (MMICs) for the generation of MMW signals. We investigate the maximum output power of these devices and compare the phase noise of MMW signals generated by UTC-PDs and InP HEMT MMICs. We describe the antennas we used and their operation technologies. Finally, we investigate the dependence of transmission distance on availability using the statistical rain attenuation data. The calculation results show that the 120-GHz-band wireless link can transmit 10-Gbit/s data over a distance of 1 km with availability of 99.999%.**

***Index Terms*—Broadband communications, high-electron mobility transistor (HEMT), millimeter-wave radio communications, photodiode.**

I. Introduction

BROADBAND wireless link using the upper millimeter-wave (MMW) band has recently been attracting significant interest among a diverse group comprising telecommunications carriers, mobile telephone and data network operators, broadcasters, consumer electronics manufacturers, enterprise users, and others, because of its gigabit-class data transmission capability. For indoor applications, gigabit-class 60-GHz-band wireless standards, such as WirelessHD and IEEE802.15.3c, have been established, and a WirelessHD system has achieved 4.0 Gbit/s and already been integrated into television systems [1]. For outdoor applications, TV program relay broadcast and high-speed backhaul services for mobile communications appear to be the most promising applications, because the data rate necessary for these applications is increasing in proportion to the broadband trend in high-definition video or new mobile services. The 60-GHz-band and *E*-band wireless link can achieve a data rate from 1.0 to 2.5 Gbit/s, and they have been actually used in the mobile backhaul services. It is expected that the over-10-Gbit/s data rate will be required for mobile backhaul in the near future.

To achieve a 10-Gbit/s data rate, we have been developing a 120-GHz-band MMW wireless link. The 120-GHz band is an unexplored frequency region in the field of industries, and the absorption coefficient of air is relatively small (about 1 dB/km), compared with a higher frequency region. Therefore, the 120-GHz-band wireless link is suitable for broadband outdoor fixed wireless systems, and we have succeeded in the outdoor transmission of 10-Gbit/s data [2].

The transmission distance and the availability are very important for TV relay broadcast and mobile backhaul applications. In order to increase the transmission distance and availability, we need to increase the output power of the wireless transmitter and decrease the received power necessary for error-free transmission. However, it has been difficult to generate high-power radio signals due to the limitations of semiconductor devices, because semiconductor device characteristics deteriorate as the operation frequency increases. We have used a high-speed uni-traveling carrier photodiode (UTC-PD) [3] and InP high-electron mobility transistor (HEMT) millimeter-wave monolithic integrated circuits (MMICs) [4], both developed by us. An evaluation of rain attenuation is also important for estimating availability, because rain attenuation of 120-GHz-band MMW is large.

This paper presents our progress in 120-GHz-band wireless system technologies that contribute to extending the transmission distance of the wireless links. Section II describes the progress in the transmission distance and the technologies we used. Section III explains the devices we use to generate 120-GHz-band radio signals and discusses the possibility of obtaining maximum output power from these devices. Section IV covers the technologies we use to decrease the received power necessary for error-free transmission, such as forward error correction (FEC), and low-noise amplifiers (LNAs). Section V describes the antennas we have used and describes a system for auto-alignment of antenna direction in 120-GHz-band wireless links. Section VI describes in detail our two 120-GHz-band wireless link systems, one of which uses the UTC-PD and other HEMT MMICs, and compares their features. Section VII discusses the transmission distance and availability on the basis of statistical data, such as the cumulative distribution of rain rate and rain attenuation of 120-GHz-band MMWs, obtained in long-term outdoor transmission experiments. Section VIII concludes the paper.

Manuscript received June 29, 2011; revised November 15, 2011; accepted November 17, 2011. Date of publication January 12, 2012; date of current version March 02, 2012. This work was supported in part by the Research and Development Project for the Expansion of Radio Spectrum Resources, of the Ministry of Internal Affairs and Communications, Japan.

A. Hirata, H. Takahashi, J. Takeuchi, H. Togo, M. Yaita, N. Kukutsu, K. Aihara, and Y. Sato are with NTT Microsystem Integration Laboratories, NTT Corporation, Kanagawa 243-0198, Japan (e-mail: hirata.akihiko@lab.ntt.co.jp).

T. Kosugi and K. Murata are with NTT Photonics Laboratories, NTT Corporation, Kanagawa 243-0198, Japan.

T. Nagatsuma is with the Graduate School of Engineering Science, Osaka University, Osaka 560-8531, Japan.

Y. Kado is with Kyoto Institute of Technology, Kyoto 606-8585, Japan.

Digital Object Identifier 10.1109/TMTT.2011.2178256

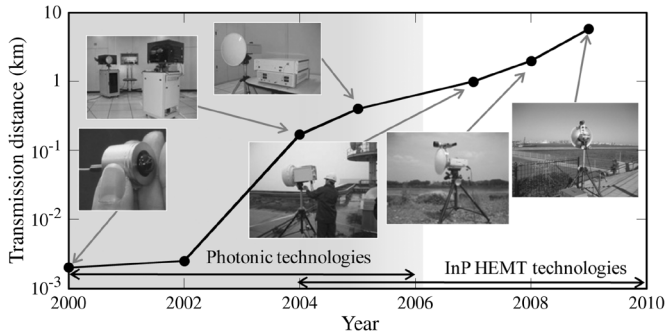

Fig. 1. Progress in the transmission distance of the 120-GHz-band wireless link.

II. Progress of the 120-GHz-Band Wireless Link System: Transmission Distance

Fig. 1 shows the transmission distance of the 120-GHz-band wireless link. Photographs of the wireless equipment used for the transmission experiments are also shown. At the early stage (2000–2005), the 120-GHz-band wireless signals were generated by photonic technologies, because photonics technologies have broadband characteristics and are suitable for generating high-frequency signals. Moreover, we can modulate MMW signals at a rate of over 10 Gbit/s because we can use high-speed optical Mach–Zehnder modulators in the photonic MMW generation systems. Data transmission over a distance of 2 m at 1.25 Gbit/s was achieved in 2000 [5], [6], and the world's first 10-Gbit/s data transmission over a radio wireless link was accomplished in 2002 [7]. We used planar antennas in those two experiments. In 2003, we started working on the MMICs for the 120-GHz wireless system. Component circuits, i.e., LNAs, power amplifiers (PAs), modulators, and demodulators, were designed and improved to ensure long-range transmission. PAs and LNAs were implemented to enhance performance of the photonic system. We obtained the first experimental radio station license from the Ministry of Internal Affairs and Communications of Japan in 2004 and conducted the first outdoor transmission experiments over a distance of 170 m [8]. At that stage, 120-GHz-band MMW amplifiers and high-gain antennas, such as Gaussian optic lens antennas or Cassegrain antennas, were introduced into both the transmitter and receiver, which made the outdoor transmission experiments possible.

Since 2007, we have been generating the 120-GHz-band wireless signals using InP HEMT MMIC technologies [2]. The InP HEMT MMICs have a narrow operation bandwidth compared with photonic technologies; however, all-electronic systems have advantages of compactness and low cost, especially when the transceiver functions are implemented with MMICs. The wireless equipment was designed to be weatherproof, which makes it possible to conduct long-term outdoor transmission experiments. In 2009, 5.8-km 10-Gbit/s data transmission was achieved in fine weather by increasing the output power and antenna gain and by introducing FEC technologies [9].

As shown in Fig. 1, the transmission distance increased from 2 m to 5.8 km in nine years, mainly due to improvements in output power, receiver sensitivity, and antenna gain. We describe the characteristics of these devices we used in the following sections.

III. Output Power of Devices Used for Generating the 120-GHz-Band Wireless Signals

Here, we discuss the 120-GHz-band wireless link output power and investigate the maximum output power that can be obtained by the devices we have used (UTC-PDs or InP HEMTs) in the 120-GHz band.

Gunn oscillators, impact oscillators, and backward oscillators (BWO) had been studied as generators of over-100-GHz signal [10]–[12]. These devices can generate over 10 dBm of output power at frequencies above 100 GHz. However, it was difficult to apply these devices for wireless communications because they lacked the characteristics required for telecommunications applications, such as high-frequency stability, frequency tunability, and low phase noise. In particular, the lack of high-speed modulation was a big obstacle to wireless communications applications.

Photonic technologies enable us to generate MMW signals at over 100 GHz with conventional photonic devices, and it is possible to modulate MMW signals at a rate of 10 Gbit/s by using optical modulators. Key devices for the generation of over-100-GHz MMW signals are a high-power and high-speed O/E convertor and a low-phase-noise photonic MMW source. We used a UTC-PD as a high-power and high-speed O/E convertor [3]. The UTC-PD uses only electrons as its active carriers, and its prime feature is high current operation.

On the other hand, recent technological progress in semiconductor devices has been remarkable. This is especially true for compound semiconductor transistors, such as HEMTs and heterojunction bipolar transistors (HBTs), which are attracting a great deal of interest because of their high-speed characteristics. Recent improvements in electron beam gate lithography are seeing the speed of HEMTs increase as the gate length decreases, and InP HEMTs with maximum oscillation frequency $(\mathrm{f_{max}})$ of over 1 THz have already been developed [13]. These transistors enable us to make electronic devices that operate at frequencies over 100 GHz.

The transitions in the output power of the 120-GHz-band wireless link are shown in Fig. 2, where the output power is the average power of the ASK-modulated MMW signal output from the transmitter. We used UTC-PDs for the transmitter before 2002, and the output power ranged from about 0 to 7 dBm. Later, we used an InP HEMT MMIC amplifier as a post-amplifier of UTC-PD output and were able to increase the output power up to 10 dBm. Since 2007, we have generated the 120-GHz-band MMW signal with a frequency multiplier and amplifiers made of InP HEMT MMICs, and we have achieved 16-dBm output power using composite-channel (CC) InP HEMT MMICs with improved breakdown voltage [14].

Next, we investigated the saturation output power of the UTC-PD at a frequency of 125 GHz. Critical current $I_{\max}$ of the UTC-PD can be approximated as

$$I_{\max} = Sqn_C v_s^{\mathrm{electron}} \quad (1)$$

$$n_C = 2\varepsilon \left[-V_{pd} + V_{bi} - E_C^{\mathrm{electron}} W_C\right] / \left(qW_C^2\right) \quad (2)$$

where W_C is depletion width, n_c is critical electron density, S is junction area, R_L is load resistance, v_s^{electron} is electron overshoot velocity, ε is dielectric constant, V_{pd} is voltage applied to

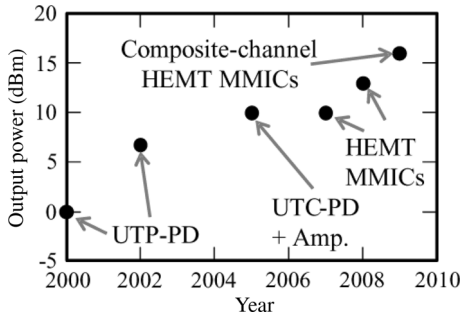

Fig. 2. Changes in output power of the 120-GHz-band transmitter.

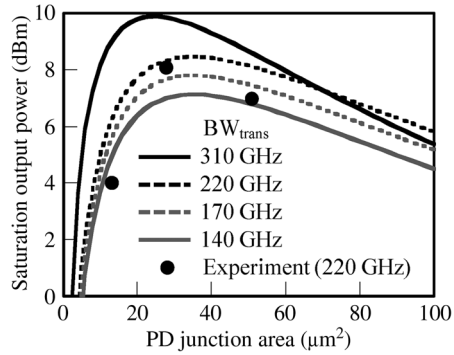

Fig. 3. Dependence of saturation output power on the PD junction area.

the PD, $V_{\rm op}$ is operation voltage (-3.0 V), $V_{\rm bi}$ is built-in voltage (0.75 V), and $E_C^{\rm electron}$ is critical electron field (50 kV/cm) [3].

When the load of UTC-PD is R, the relationship between $V_{\rm pd}$ and $V_{\rm op}$ can be approximated as

$$V_{\rm op} = V_{pd} + RI. \tag{3}$$

Therefore, $I_{\rm max}$ of the UTC-PD can be approximated as

$$I_{\rm max} = \frac{V_{\rm op} - V_{\rm bi} + E_C^{\rm electron} W_C}{R_L + \frac{Wc^2}{2\varepsilon S v_s^{\rm electron}}}. \tag{4}$$

The frequency characteristics of the UTC-PD output power are determined by the *RC* time-constant-limited bandwidth ($BW_{\rm CR}$) and the carrier-transit-time-limited bandwidth ($BW_{\rm Trans}$). We investigated the effect of junction capacitance on the UTC-PD output power at a frequency of 125 GHz. Junction capacitance C_{j0} is expressed as

$$C_{j0} = \frac{S\varepsilon}{W_C}. \tag{5}$$

The ratio of UTC-PD output power at an operation frequency of f over the output power during dc operation (α) is given by

$$\alpha = \left| \frac{1}{1 + (2\pi f R(C_{j0} + C_p))^2} \right| \times \left| \frac{1}{1 + \left(\frac{f}{BW_{\rm trans}}\right)^2} \right| \tag{6}$$

where f is operation frequency and C_p is parasitic capacitance. The effect of UTC-PD series resistance is ignored for simplicity.

Therefore, the saturation output power $\rm P_{sat}$ is given by

$$P_{\rm sat} = \frac{\alpha R I_{\rm sat}^2}{8}. \tag{7}$$

We calculated the junction area dependence of UTC-PD saturation output power using (7). The calculation result is shown in Fig. 3. We set the $v_s^{\rm electron}$ constant (4×10^7 cm/s) to simplify the simulation of saturation output power, even though, in reality, $v_s^{\rm electron}$ changes with $V_{\rm pd}$. For a UTC-PD with a $BW_{\rm Trans}$ of 220 GHz (W_C: 290 nm), maximum output powers of about 8 dBm are obtained with a junction area of about 30–40 μm^2. On the other hand, a maximum output power of about 10 dBm can be obtained when $BW_{\rm Trans}$ is 310 GHz (W_C: 230 nm), and the junction area is about 25 μm^2. We measured the maximum output power of UTC-PDs on-wafer with $BW_{\rm Trans}$ of 220 GHz at a frequency of 125 GHz using a power meter connected to a MMW probe. The measurement results are also shown in Fig. 3. The maximum output powers are 4.0, 8.1, and 7.0 dBm for junction areas of 13, 29, and 50 μm^2, respectively. The measured power qualitatively coincides with the simulation results.

Ito *et al.* showed that the output power of the UTC-PD can be increased by using a matching circuit, and they obtained 13.6 mW at 100 GHz [15]. We applied this technique for the 120-GHz-band wireless link. Fig. 4(a) is the schematic of the equivalent circuit. We measured the S-parameter and current–voltage characteristics of the UTC-PD to obtain the equivalent circuit model of UTC-PD. For the calculation, we used the junction area and $BW_{\rm Trans}$ of the PD of 23 μm^2 and 220 GHz, respectively. A resonant matching circuit composed of a short stub circuit compensates for the imaginary part of internal impedance in the UTC-PD at a specific frequency. On the other hand, introducing the resonant matching circuit makes the UTC-PD operation bandwidth narrow. The matching condition can be changed by setting the length of transmission line L_a and that of short stub L_b shown in Fig. 4(a). The simulation results for PDs (PDa-PDe) with matching circuits with different L_a and L_b are shown Fig. 4(b). Table I shows the L_a and L_b of UTC-PDs with a matching circuit. The relative response in the narrowband design at 125 GHz is about 45% to 130% higher than that for the UTC-PD without the matching circuit. On the other hand, there is a tradeoff between the maximum output power and bandwidth. For 10-Gbit/s data transmission using an ASK modulation scheme, the bandwidth of the devices should be about 17 GHz. Fig. 4(c) shows the relationship between the peak power and bandwidth. For PDe, which achieves highest peak power (15 mW), the 1-dB bandwidth is 8 GHz, which is insufficient for 10-Gbit/s data transmission. To obtain the bandwidth of over 17 GHz with a margin, we selected PDb. Fig. 5 shows the measurement results for PDb at 125 GHz. The output power of a PD without a matching circuit is also shown. PDb with a matching circuit exhibits 50% higher efficiency than the one without it, which coincides with the simulation results in Fig. 4(c).

These results indicate that a UTC-PD itself can generate about 10 dBm at 125 GHz. However, linearity is required for ASK systems, and 3-dB back-off is required for the ASK modulation scheme; therefore, we have to use a UTC-PD with an output power of a few dBm. One way to obtain over 10 dBm

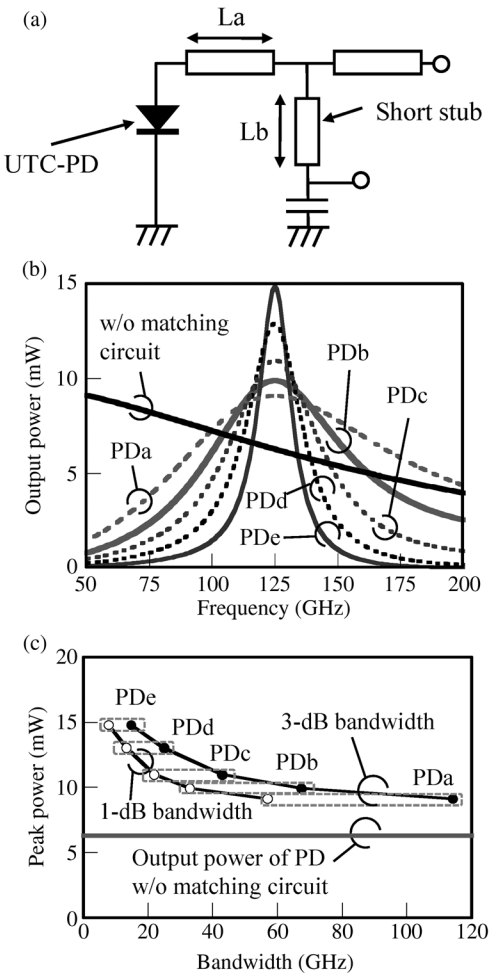

Fig. 4. (a) Schematic of the equivalent circuit of a UTC-PD with a matching circuit, (b) simulated UTC-PD output power, (c) simulated relationship between 1-dB bandwidth and peak power.

TABLE I
L_a AND L_b OF UTC-PDs WITH A MATCHING CIRCUIT

	L_a (μm)	L_b (μm)
PDa	13	134
PDb	53	97
PDc	75	74
PDd	95	54
PDe	113	35

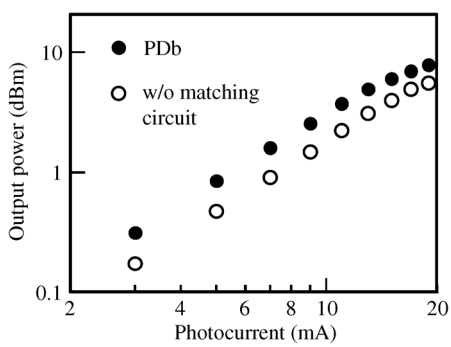

Fig. 5. Measured output power of UTC-PDs with and without matching circuit at 125 GHz.

of output power in the 120-GHz band is to introduce of a PA, which we investigate next.

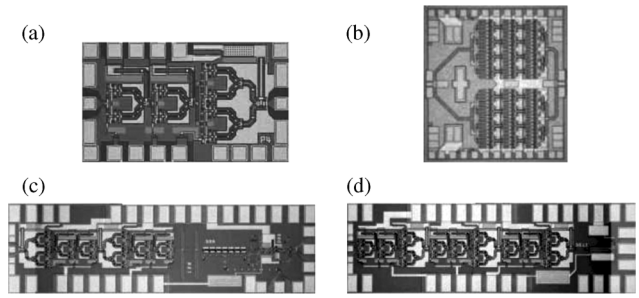

Fig. 6. Photographs of InP HEMT MMICs. (a) PA using conventional InP HEMT. (b) PA using CC InP HEMT MMICs. (c) Tx MMIC using conventional InP HEMT. (d) Rx MMIC using conventional InP HEMT.

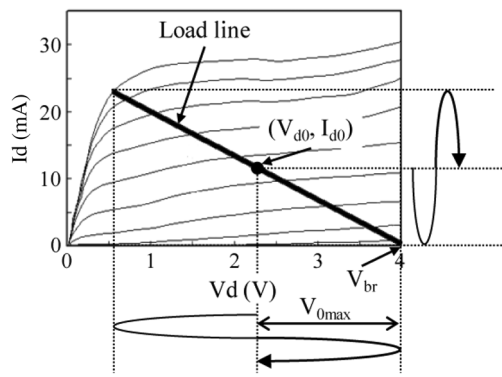

Fig. 7. Typical current–voltage characteristics of a fabricated 0.8-μm-gate CC HEMT with gate width of 40 μm.

InP HEMT MMICs feature high-speed and high-power operation, and we have succeeded in making PAs that employ an InP HEMT MMIC [4]. A photograph of the PA MMIC chip is shown in Fig. 6(a). The chip size is 1.0 mm × 2.0 mm. We investigate the output power of the InP HEMT MMIC PA that operates at a frequency of 120 GHz. The bias point has a major impact on a PA's output power. The effect of the bias point can be obtained by considering the device's current–voltage (I–V) characteristic in conjunction with a load line. The maximum output power can be obtained when the load line allows maximum voltage and current excursion. The most effective way to increase the maximum voltage excursion is to increase the breakdown voltage of the InP HEMTs. The use of an InGaAs/InP composite channel (CC) is effective for increasing the breakdown voltage while maintaining high-frequency performance. The 0.08-μm-gate CC InP HEMT we have developed typically have a unity current gain frequency f_t of 180 GHz and a maximum oscillation frequency $f_{\max}$ of 580 GHz [16]. Fig. 7 shows typical dc current–voltage characteristics of 0.08-μm-gate CC HEMTs at room temperature. The gate width is 40 μm. The off-state breakdown voltage of the HEMTs is around 10 V, and reliable operation can be expected below 4.0 V from the results of bias temperature acceleration tests. These values are almost two times higher than those of conventional lattice-matched InP-HEMTs.

The output power of an HEMT is expressed as

$$P_{\text{out}} = \frac{1}{T}\int_0^T \left[\{V_{d0} - V_d(t)\} \times \{I_{do} - I_d(t)\}\right] dt \qquad (8)$$

where the bias point is (V_{d0}, I_{d0}) and $V_d(t)$ and $I_d(t)$ are drain voltage and drain current that swing on the load line, respectively. Maximum voltage excursion can be obtained when we set the bias point $(V_{d0}, I_{d0}) = (2.25\ \text{V}, 12\ \text{mA})$, and $V_{d(t)}$ is expressed as

$$V_d(t) = V_{o\,\max} \cdot \sin\left(\frac{2\pi}{T}t\right) = (V_{br} - V_{do}) \cdot \sin\left(\frac{2\pi}{T}t\right) \quad (9)$$

where V_{0max} is voltage swing and V_{br} is breakdown voltage.

The output power of one HEMT calculated by (8) and (9) is about 10 dBm. This calculation is based on a dc load line analysis and is different from the actual ac behavior of the HEMT. The transconductance (gm) of the HEMT decreases at both ends of the load line; therefore, we have to limit the voltage swing to avoid nonlinear operation of the PA. Judging from the drain voltage dependence of gm, $V_{0\,\max}$ should be below 1.0 V and the bias point $(V_{d0}, I_{d0}) = (2.0\ \text{V}, 13\ \text{mA})$ for linear operation. The $P_{1\ \text{dB}}$ output power of the HEMT calculated using these values is about 5.4 dBm.

We fabricated a PA MMIC using the CC InP HEMTs [14]. The photograph of the PA MMIC using CC InP HEMTs is shown in Fig. 6(b). The chip size is 2.0 mm $\times$ 2.2 mm. The amplifier has a three-stage common-source configuration. To increase total power handling capability, we divided the amplifier into eight medium-power amplifiers (MPAs) with an on-chip power divider (eight-way) and combiner (eight-way). Each MPA handles only one-eighth of the total RF and dc power. Therefore, narrow transmission lines with a high cut-off frequency and low radiation loss can be used in the cuircuit design. Over 100 HEMTs with a gate width of 30 μm were used at the final stage of the PA circuits, and these HEMTs were combined with a power combiner circuit. The total $P_{1\ \text{dB}}$ output power calculated from the number and gate width of the HEMTs at the final stage is approximately 25 dBm. We fabricated a PA module by integrating the PA MMICs in a metal package [14]. The photograph of the PA module is shown in Fig. 8(a). The thickness of the PA MMIC chip integrated in a metal package was 0.15 mm. The output of the MMIC was transmitted to the waveguide via a waveguide-to-planar-circuit transition. The MMIC and waveguide-to-planar-circuit transition were connected by wire bonding. Details of the waveguide-to-planar-circuit transition and MMIC integration are shown in [17]. The efficiency of the PA MMIC was below 5%. The $P_{1\ \text{dB}}$ output power of the PA module is about 19 dBm, and the saturation output power is about 21 dBm at 125 GHz. There is a 6-dB difference between the PA module $P_{1\ \text{dB}}$ output power and the calculated PA MMIC $P_{1\ \text{dB}}$ output power. We suppose that the difference is due to loss at the power combiner in the PA MMIC and at the waveguide-to-planar-circuit transition in the PA module. When we use the PA module for an ASK-modulation wireless transmitter, the average power of the transmitter should be 16 dBm for linear operation. From the viewpoint of chip area and power consumption, the number of HEMTs at the final stage can be more than doubled. We think that the Tx with ASK modulation scheme can achieve about 20-dBm $P_{1\ \text{dB}}$ average output power by using this CC InP HEMT MMIC.

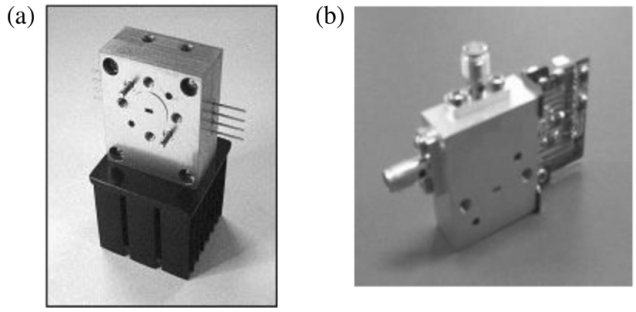

Fig. 8. Photograph of (a) Rx and Tx module, and (b) PA module. The package of Tx module and Rx module are same.

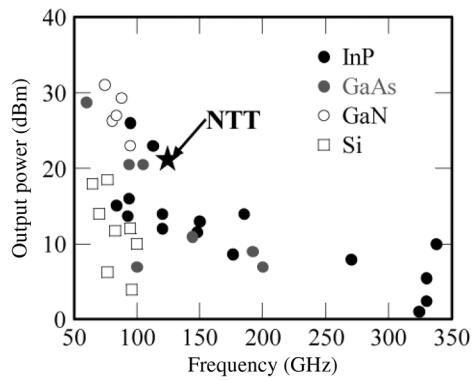

Fig. 9. Maximum output power of MMW PAs.

We compare the maximum output power of reported PAs in Fig. 9. GaN devices achieve the highest power at frequencies below 100 GHz. Micovic *et al.* reported a GaN HEMT PA MMIC whose maximum output power is 29.3 dBm at 88 GHz [18]. At frequencies above 100 GHz, InP HEMT devices show higher output power than other devices at the same operation frequency. Deal *et al.* reported an InP HEMT PA MMIC with an output power of 8 dBm at 270 GHz [19]. Our PA has the highest output power in the 120-GHz band, and the output power of our PA coincides with the trend in the relationship between the maximum output power and the operation frequencies.

For the generation of 125-GHz-band signal that is amplitude-modulated at a data rate of 10 Gbit/s, we have developed a transmitter (Tx) MMIC using the standard InP HEMT technologies [4]. In the transmitter MMIC, a frequency multiplier, ASK modulator, and amplifiers are integrated in one chip. The photograph of the transmitter MMIC is shown in Fig. 6(c). The chip size is 1.0 mm $\times$ 3.0 mm. The transmitter MMIC can generate over 0-dBm 125-GHz-band MMW signal that is ASK modulated at a rate of up to 11.1 Gbit/s. We have developed a Tx module that integrates a Tx MMIC chip in a metal package, as shown in Fig. 8(b) [17].

IV. Receiver Technologies

The 120-GHz-band wireless link employs an envelope detection method using Schottky barrier diodes (SBDs). Fig. 10 shows the transition in receiver sensitivity. At first, we used a conventional waveguide MMW detector, which had a video

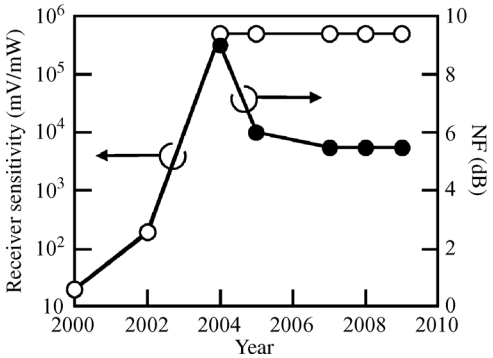

Fig. 10. Transition in the sensitivity of the 120-GHz-band receiver.

sensitivity of 10^3 mV/mW when the video load impedance was 1 MΩ. However, we had to set the video load impedance to 50 Ω for high-speed data transmission, which decreased the video sensitivity to 20 mV/mW. We then developed a planar broadband receiver with SBDs and a planar slot ring antenna [6]. The SBD chip was flip-chip bonded on the planar slot ring antenna chip made on a Si substrate. With optimized data output circuits, the receiver achieved a video sensitivity of 190 mV/mW at a load impedance of 50 Ω.

In order to improve the video sensitivity of the receiver, we developed a receiver MMIC chip that monolithically integrates HEMT detector and an LNA [4]. The photograph of the receiver MMIC is shown in Fig. 6(d). The chip size is 1.0 mm × 3.0 mm. The video sensitivity of the HEMT detector itself is about 400 mV/mW, and with the integration of an LNA with a gain of 33 dB, the sensitivity of the receiver MMIC chip reached 5×10^5 mV/mW.

For the wireless data transmission, it is important to increase the C/N ratio at the receiver. In a wireless transmission system with ASK modulation and envelope detection, a C/N ratio of over 20 dB is necessary for a bit error rate (BER) of 10^{-12} [20]. Noise power at the receiver $(N_{\rm thr})$ mainly comes from the thermal noise of the LNA, which is given by

$$N_{\rm thr} = k_b T \bullet NF_r \bullet \Delta f \tag{10}$$

where k_b is Boltzmann's constant, NF_r is the noise figure (NF) of the amplifier in the receiver, and Δf is the bandwidth of the amplifier.

One way to increase the C/N ratio is to improve the NF of the LNA. Fig. 10 shows how the NF has changed for the 120-GHz-band LNA. The NF of the LNA was about 9 dB at first, and it was decreased to 5.6 dB by using a combination of two kinds of matching circuits [21]. We have developed a receiver (Rx) module that integrates an Rx InP HEMT MMIC chip composed of HEMT detector and LNA [Fig. 8(b)] [17]. Introducing a bandpass filter (BPF) in the Rx MMIC chip is effective for increasing the C/N ratio. For this purpose, we employed a planar BPF composed of two dual coplanar open stubs [4]. The $N_{\rm thr}$ becomes −65.2 dBm when the NF is about 5.6 dB and Δf is 20 GHz. Therefore, the theoretical received power necessary for a BER of 10^{-12} is −43.6 dBm.

We can reduce the required C/N ratio necessary for the data transmission with a BER of 10^{-12} by using FEC technologies. Many kinds of FEC methods, such as low-density parity-check (LDPC) code, BHC code, and punctured code, have been used in various wireless communications systems. On the other hand, several requirements must be met for the application of FEC to the 120-GHz-band wireless link. One of the promising applications of the 120-GHz-band wireless link is live relay broadcast of uncompressed high-definition videos, for which FEC should be able to handle high-speed data with a small latency. Therefore, we selected Reed–Solomon (RS) coding because it satisfies the above requirements. For example, the latency due to FEC should be below one frame of the television signal (below 33 msec) for the transmission of uncompressed high-definition videos in order to keep synchronization between different video signals. The latency of FEC using RS coding is below 10 μs, and this value satisfies our requests. FEC using RS coding has already achieved 10-Gbit/s data rate in the optical transport network (OTN). Moreover, FEC using RS coding can obtain coding gain of about 6 dB at a BER of 10^{-12} with small increase of data rate (about 7%) [22].

Another way to reduce the required C/N ratio is to change the modulation scheme. The BPSK modulation scheme requires a lower C/N ratio than the ASK modulation scheme. We developed a BPSK modulation module and demodulation module, and a back-to-back test showed that these modules can transmit 10-Gbit/s data with lower received power than ASK modules [23].

Fig. 11 shows the relationship between the BER and the received power of the wireless link at 10 Gbit/s. The BERs were measured by a free-space transmission experiment (Exp. 1) and back-to-back tests (Exp. 2–4). In experiment 1 (Exp. 1), the transmitter used a photonic emitter with a UTC-PD, and the receiver was a planar broadband receiver composed of SBDs and a planar antenna [5]. MMW amplifiers were not used in the transmitter and receiver, and about −3-dBm received power is required for a BER of below 10^{-12}. In experiment 2 (Exp. 2), as a transmitter, we used a photonic waveguide module that integrated a UTC-PD chip and PA chip and used an Rx waveguide module as a receiver [8]. The use of an MMW amplifier at both of transmitter and receiver reduces the received power necessary for a BER of 10^{-12} to about −30 dBm. In experiment 3 (Exp. 3), we used a Tx module and a PA module as a transmitter and used an Rx module as a receiver, in which a Rx MMIC chip with a BPF and an NF-improved LNA were integrated [2]. The bandwidth limitation by the BPF and the NF improvement of LNA contributed to considerably reduce the received power necessary for a BER of 10^{-12} to about −40 dBm. This value is 3.6 dB higher than the theoretical value discussed above with (10).

When we used RS (255,239) coding defined in the ITU-T Recommendation G.709 Interfaces in the same transmitter and receiver setup as in Exp. 3, a BER of 10^{-12} was obtained when the received power was about −46 dBm (Exp. 4) [9]. This value is about 43 dB lower than that in Exp. 1, in which neither an LNA nor FEC were not employed.

V. Antenna Technologies

For the 120-GHz-band wireless link, the output power is generally smaller than that of microwave wireless systems

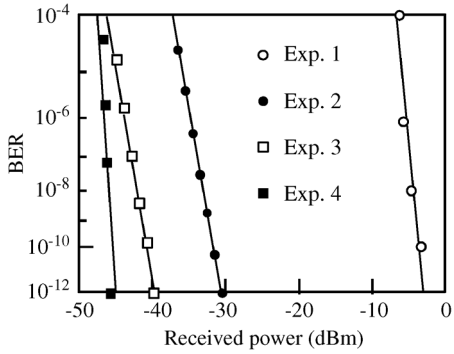

Fig. 11. Relationship between the BER and received power of the wireless link at 10 Gbit/s.

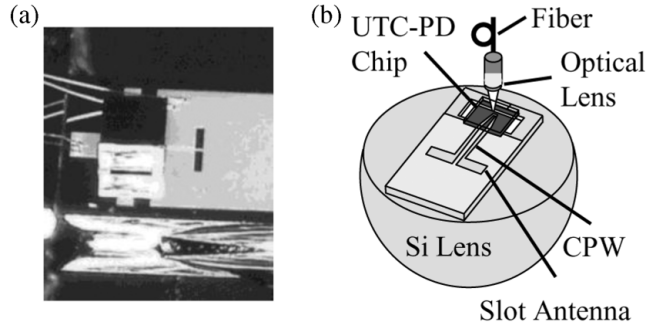

Fig. 12. (a) Photographs of planar antennas used for the 120-GHz-band wireless link. (b) Schematic of photonic MMW transmitter module using planar slot antenna.

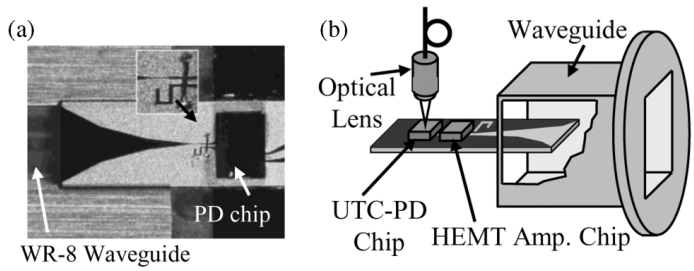

Fig. 13. (a) Photograph of planar-circuit-to-waveguide transition on a Si substrate. (b) Schematic of photonic MMW transmitter module that employs planar-circuit-to-waveguide transition.

due to the limitation of generator characteristics, as discussed in Section III. Moreover, the received power necessary for error-free transmission is higher than that of microwave systems, because 120-GHz-band wireless system requires a broad bandwidth for the transmission of 10-Gbit/s data. Moreover, the free-space transmission loss is large due to the short wavelength. Therefore, we need to use high-gain antennas to transmit data over a distance of 1 km.

At a 120-GHz-band frequency, the reduction of transmission loss between the transmitter/receiver chip and the antenna is important. Therefore, we developed a planar antenna on which a PD is hybridly or monolithically integrated [24]–[26].

Fig. 12(a) is a photograph of the planar slot antenna on which a UTC-PD chip is flip-chip bonded, and Fig. 12(b) shows the diagram of the designed photonic MMW transmitter using the planar slot antenna [24]. The transmitter consists of a planar antenna chip, a UTC-PD chip, a hemispherical Si lens, and an optical fiber with a collimating lens. We used a coplanar waveguide-fed (CPW-fed) slot antenna for the planar antenna chip because it has an antenna pattern perpendicular to the substrate and is suitable for the connection of planar-active devices. The slot antenna and the CPW were formed on a Si substrate ($\varepsilon r = 11.7$), which was 0.4 mm thick. To decrease the dispersion and radiation loss due to the substrate, we used high-resistivity Si and thick gold. The resistivity of the Si was 1 k$k\Omega$cm, and the thickness of the gold was 10 μm. The antenna gain obtained by a 3-D electromagnetic simulation based on the finite-element method (FEM) was about 13.5 dB. In the data transmission experiments, Teflon lenses with a diameter of 50 mm were used to collimate the output of the planar antenna. The output power of the transmitter was -3 dBm at a frequency of 120 GHz, and we have succeeded in the transmission of 10-Gbit/s data over a distance of 2 m by using a Teflon lens to collimate the MWW beam [7].

However, antenna gain of over 40 dBi is necessary for the 120-GHz-band wireless link to transmit 10-Gbit/s data over a distance of 1 km, and the gain of these antennas shown in Fig. 12 is insufficient.

A Gaussian optic lens antenna (GOA) and Cassegrain antenna (CA) have high gain, and both have a waveguide port. Therefore, it was necessary to develop a planar-circuit-to-waveguide transition in order to use these high-gain antennas.

Fig. 13(a) shows a photograph of planar-circuit-to-waveguide transition made on a Si substrate, and Fig. 13(b) is a schematic of photonic MMW transmitter module that employs the planar-circuit-to-waveguide transition. [9]. We selected Si substrate because we can use the matured and low-cost Si fabrication process. A UTC-PD chip is flip-chip bonded on a planar-circular chip. The MMW signals travel along a CPW to a tapered slot antenna inserted into the waveguide. The thickness of the Si substrate was set to 100 μm to reduce the effect of surface waves. Optical MMW signals are input to the UTC-PD from the backside, and the UTC-PD converts them into MMW signals. The MMW signals travel along a coplanar waveguide (CPW) to a tapered slot antenna inserted into the waveguide.

Fig. 14 shows the simulated S-parameter of the planar-circuit-to-waveguide transition. We employed the finite element method (FEM) for the simulation. The input port is the CPW, and the output port is the waveguide. The insertion loss improves as the substrate gets thinner; it is below 2 dB when the substrate is 100 μm thick at a frequency of 90–140 GHz.

We also developed a planar-circuit-to-waveguide transition made on a quartz substrate to reduce the transmission loss [17]. The planar-circuit-to-waveguide transition is composed of a CPW-to-slotline (SL) transition, SL, and monopole antenna placed on the waveguide.

With the development of the planar-circuit-to-waveguide transition, it became possible to use high-gain GOAs and CAs. Table II shows the gain of the antennas we used for the 120-GHz-band wireless link. The GOAs have a smaller diameter than the CAs, though their gains are comparable. A standard gain horn antenna was integrated in the GOAs. The half power beamwidth (HPBW) of CAs is smaller than that

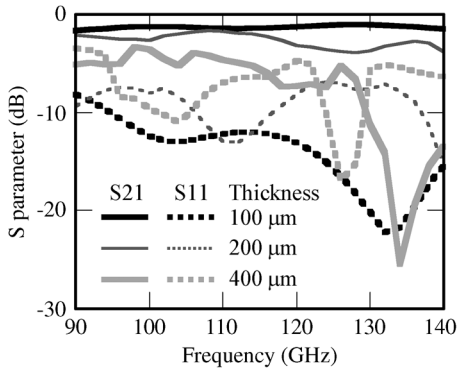

Fig. 14. Simulated S parameter of planar-circuit-to-waveguide transition that uses Si substrates with different thicknesses.

TABLE II
CHARACTERISTICS OF ANTENNAS FOR THE 120-GHz-BAND WIRELESS LINKS

	Diameter	Gain	HPBW
GOA	300 mm	49.5 dBi	0.56°
	375 mm	52.3 dBi	0.47°
CA	450 mm	48.7 dBi	0.40°
	600 mm	52.0 dBi	0.26°

of GOAs. These results indicate that the antenna efficiency of GOAs is higher than that of CAs. However, GOAs are much heavier than CAs even at similar antenna gain. Therefore, we have mainly used CAs for 120-GHz-band wireless links.

As shown in Table II, the beamwidth of the antennas is very narrow, which makes the alignment of the antenna difficult during setup. A telescope can be attached to the antenna of the 120-GHz-band wireless link, and we can make the telescope's axis direction coincide with the direction of the main lobe of the antenna. At setup, we roughly align the antenna direction manually using the telescope, then we do a fine alignment by monitoring the received power. The 120-GHz-band wireless link is unidirectional, so we have to send the received power information to the transmitter side by using some other method of wireless communications, such as a cellular phone, when the direction of the transmitter antenna is aligned. This process takes time and requires an operator with alignment experience. We therefore developed a system for auto-alignment of antenna direction. Figs. 15 and 16 show a schematic and photograph of the system, respectively. The system uses a 2.4-GHz-band wireless local area network (LAN) to send the control signal and received power information between the transmitter and receiver. The wireless LAN uses the IEEE 802.11g standard, and it can transmit 12-Mbit/s data over a distance of 10 km using a high-gain parabolic antenna. The PC at the receiver side controls the motion of the antenna platforms of the transmitter and receiver alternately to maximize the received power at the receiver. The PC at the receiver side calculates the received power from the monitor voltages output from the receiver.

Fig. 17 shows the scanning algorithm of auto-alignment program. The auto-alignment program consists of a coarse alignment step and a fine alignment step. We can change the scanning area in the coarse alignment step. In Step 1, the Rx antenna scans coarsely as shown in Fig. 17. When no MMW power is detected by Rx during coarse scanning, the direction of Tx

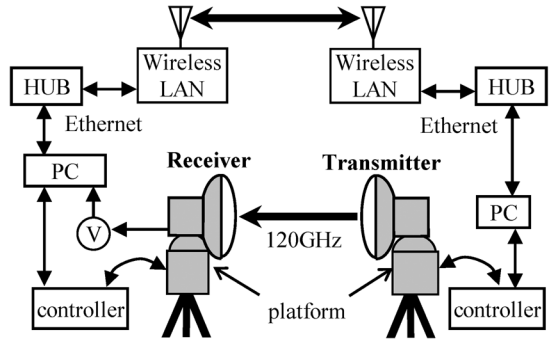

Fig. 15. Schematic of the auto-alignment system.

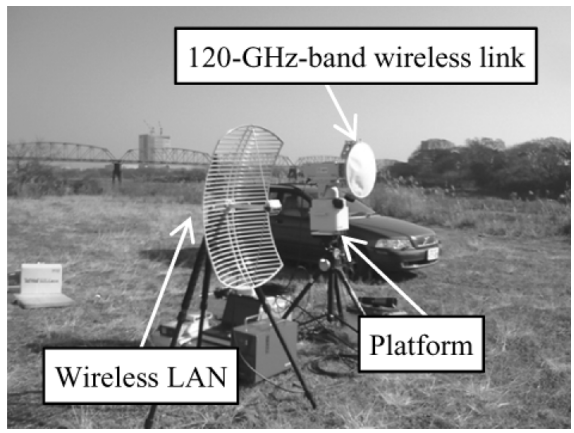

Fig. 16. Photograph of the auto-alignment experiment (transmitter).

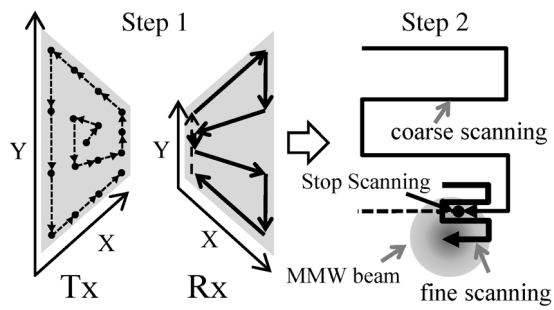

Fig. 17. Scanning algorithm of auto-alignment system.

antenna moves to the next position, then the Rx antenna starts coarse scanning. When MMW power is detected by Rx, the program moves to Step 2. The coarse scanning of Rx antenna stops when MMW power is detected, and fine scanning of Rx antenna starts. When the fine scanning finishes, Rx antenna moves to the position that maximum received power was obtained during fine scanning. After that, Tx antenna starts fine scanning, and moves to the position that maximum received power was obtained during fine scanning.

Fig. 18 shows the time necessary for auto-alignment. In the experiment, we set the transmitter and receiver 1 km apart. First, we aligned both the transmitter and receiver antenna directions to obtain the maximum received power, then we shifted both the transmitter and receiver antenna directions by a certain offset angle. At this stage, we started the auto-alignment program. We set the scanning area to be $\pm 1.5°$. The system achieves

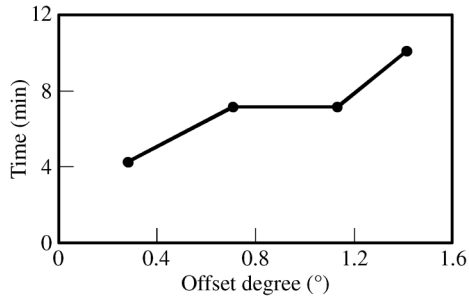

Fig. 18. Dependence of time necessary for auto-alignment on the offset angle of the antenna.

auto-alignment in a 4–10 min when the offset angle is below 1.4°. This is comparable to the time it takes experienced operator to align the antennas. When offset angle is over 1.7°, the auto-alignment system does not converge, because we set the coarse scanning area to be $\pm 1.5°$. The antenna direction can be aligned manually within $\pm 1.5°$ from the right directions with the telescope. Therefore, it is possible for anyone to align the antenna direction by first aligning both the transmitter and receiver antennas using the telescope and then starting the auto-alignment program. With the auto-alignment system, the antenna directions can be aligned when the transmitter and receiver are set 1 km apart. The time for auto-alignment mainly depends on the time necessary for the first coarse scanning. We can decrease the time by increasing the speed of coarse scanning.

VI. 120-GHz-Band Wireless System

As described in Section III, we have developed two technologies for the generation of 120-GHz-band wireless signals. In this section, we present 120-GHz-band wireless systems using UTC-PD and InP HEMT MMIC technologies and compare the features of each system.

Fig. 19 shows a schematic diagram of the 120-GHz-band wireless transmitter using a UTC-PD (Tx1). The transmitter is composed of a low-phase-noise photonic MMW generator, data modulator and a UTC-PD module. In the photonic MMW generator, the output of an ultra-narrow-linewidth single-mode laser is modulated at a frequency of 62.5 GHz with a $LiNbO_3$ optical intensity modulator. The 62.5-GHz CW signals are generated by multiplying the output of a 15.625-GHz phase locked oscillator (PLO). The phase noise of PLO used in Tx1 is shown in Fig. 20. The modulated optical signals are fed into a planar lightwave circuit (PLC) that integrates an arrayed waveguide grating (AWG) and 3-dB coupler [27]. The channel spacing of the AWG is 60 GHz, and two output channels with an interval of 120 GHz are connected with the 3-dB coupler. The PLC therefore acts as an optical filter that outputs two modes whose frequency interval is 125 GHz. The output signal is amplified by an erbium-doped optical fiber amplifier (EDFA). The optical MMW signal is modulated by data signals. The modulated optical signal is amplified by the second EDFA. The amplified optical signal is input into the UTC-PD module, which is composed of a UTC-PD and an InP HEMT MMIC amplifier [28]. The optical MMW signal is O/E-converted and amplified by the UTC-PD module. The generated MMW signal is transmitted from a high-gain antenna. The 120-GHz-band wireless

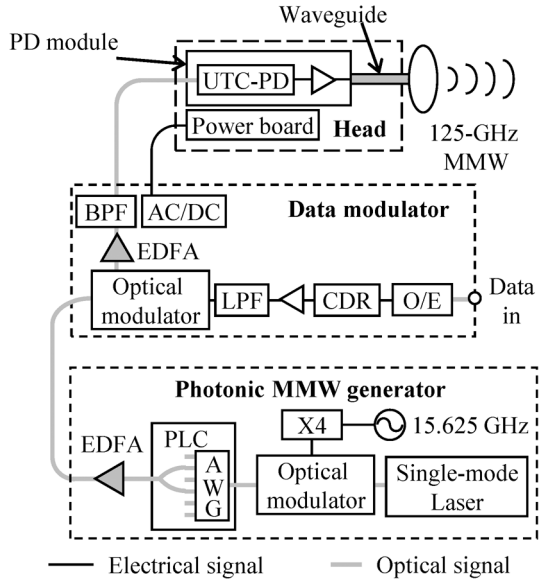

Fig. 19. Schematic of 120-GHz band wireless transmitter using a UTC-PD (Tx1).

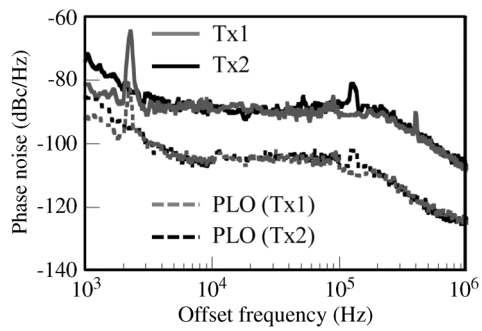

Fig. 20. SSB phase noises of down-converted 125-GHz CW signal generated by Tx1 and Tx2. SSB phase noises of PLOs used in Tx1 and Tx2 are also shown.

signals are generated in the photonic MMW generator, and the head of the wireless equipment only acts as an O/E convertor, which makes the head of the wireless equipment light and reduces its power consumption.

A schematic of the 120-GHz-band wireless receiver is shown in Fig. 21. The receiver employs a receiver module [17] with a receiver MMIC chip [4]. The photograph of the receiver (Rx) module is shown in Fig. 8(b). The receiver module amplifies the received MMW signals and demodulates them. The gain and NF of LNA used in the receiver module was 33 and 5.6 dB, respectively [4]. The demodulated data signals are amplified with a base-band amplifier. The demodulated data signals are clock-and-data recovered and converted into optical signal with an E/O converter.

Fig. 22 shows a schematic of the 120-GHz-band wireless transmitter using InP HEMT MMIC technologies (Tx2). The transmitter is composed of three components: the head, which generates the radio signal; the controller, which supplies power and the data signal and control signals to the head; and the antenna. The optical 10-Gbit/s data signals are input into the controller and transmitted to the head, where the optical data signals are O/E-converted. The transmitter uses three MMW modules:

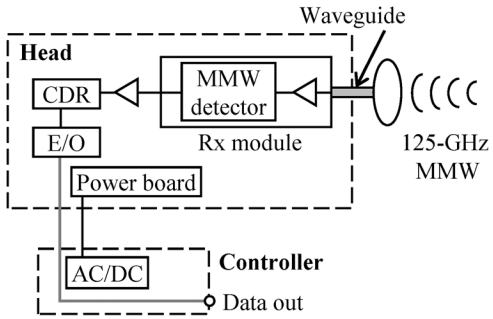

Fig. 21. Schematic of 120-GHz band wireless receiver.

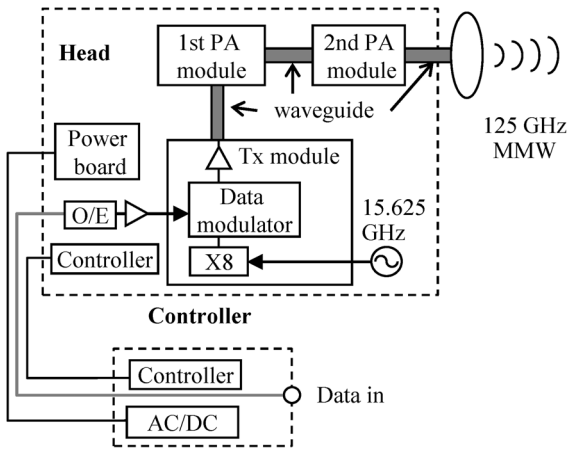

Fig. 22. Schematic of 120-GHz band wireless transmitter using InP HEMT MMICs (Tx2).

a Tx module and two PA modules [14], [17]. The photographs of PA modules and Tx module are shown in Fig. 8(a) and Fig. 8(b), respectively. The Tx module multiplies 15.625-GHz CW signal from a PLO up to 125 GHz. The phase noise of the PLO used in Tx2 is shown in Fig. 20. The ASK modulator in the Tx module modulates the 125-GHz MMW signal with 10-Gbit/s data signal, and the modulated 125-GHz MMW signals are amplified up to 0 dBm. The output of the Tx module is input to the first PA module. The first PA module amplifies the MMW signals up to 10 dBm; the second one amplifies them up to 16 dBm and outputs them to the Cassegrain antenna. The configuration of the receiver is almost the same as that shown in Fig. 21.

Table III shows the specifications of the wireless link systems using Tx1 and Tx2. The head of Tx2 is larger and heavier than the one using photonic technologies; however, the controller is much smaller than the photonic system controller (photonic MMW generator) because MMW signals are generated in the head. Moreover, the power consumption is smaller than that of the photonic systems.

Next, we compare the phase noise of the MMW signals generated by the UTC-PD with that of the signals generated by the InP HEMT MMICs. Fig. 20 shows the single sideband (SSB) phase noise of the down-converted MMW signal. The 125-GHz CW signal generated by Tx1 and Tx2 are down-converted to 5 GHz by a sub-harmonic mixer. The SSB phase noise of the PLOs used in Tx1 and Tx2 are also shown. The phase noise of the MMW signal generated by Tx1 and Tx2 are almost the same at an offset frequency of over 2 kHz, and they are about −90 dBc/Hz at an offset frequency of 100 kHz, which is larger

TABLE III
SPECIFICATIONS OF 120-GHz-BAND WIRELESS LINKS USING PHOTONIC TECHNOLOGIES (Tx1) AND InP HEMT MMIC TECHNOLOGIES (Tx2)

	UTC-PD system (Tx1)	InP HEMT MMIC system (Tx2)
Center frequency	125 GHz	125 GHz
Occupied bandwidth	116.5-133.5 GHz	116.5-133.5 GHz
Output power	10 dBm	16 dBm
Modulation	ASK	ASK
Data rate	9.953-11.096 Gbit/s	1 Mbit/s - 11.096 Gbit/s
Head size	W250×D300×H160 mm	W190×D380×H130 mm
Head weight	4.9 kg	7.3 kg
Controller size	W450×D540×H120 mm	W220×D360×H60 mm
Controller weight	20.1 kg	4.0 kg
Consumption power	<400 W	<100 W

than that of the 15.625-GHz PLO by about 18 dB. This result agrees well with the theory regarding phase noise (Phase noise is increased by 20 log(m), where m is the multiplication order [29]). The phase noise of Tx1 is smaller than that of Tx2 below 2 kHz, which is due to the phase noise difference of the PLOs used in Tx1 and Tx2. These results indicate that the phase noises of the MMW signal generated by photonic technologies and InP HEMT technologies are almost the same when the RF source (PLO) phase noise and multiplication order are the same, that the optical comb signal is coherent, and that the optical filtering process with AWGs does not affect the phase noise.

Finally, we mention the features of the wireless link using photonic technologies and InP HEMT technologies. The biggest merit of photonic technologies is that more than one radio station can share the radio signal generator. In this case, the head of the transmitter is composed of an O/E convertor and amplifier, which makes the head of the transmitter small, simple and low-cost with low power consumption. Another merit of this system is the flexibility of the wireless system. We can change the modulation scheme of the wireless link without changing the head of the transmitter. Moreover, the introduction of wavelength division multiplexing (WDM) technologies makes the construction of the multi-band wireless system possible. Multi-band radio-on-fiber (RoF) signal can be transmitted to a base station through a fiber by using WDM technologies, therefore, we can select the most suitable wireless band depending on the climate or traffic of the link. Due to these advantages, the 120-GHz-band wireless links using photonic technologies are expected to be promising for the next-generation of mobile wireless backhaul networks or indoor wireless LANs. The next-generation of mobile wireless networks will require a large number of gigabit-class base stations because the transmission distance becomes short compared with the present base stations due to the increase of transmission capacitance. On the other hand, a radio signal generator composed of conventional photonic components is more expensive and consumes more power than one that uses MMICs. In view of total system cost, the cost of a

radio signal generator per one wireless link decreases when the number of transmitters that share the radio signal generator becomes large, and the merit of wireless links using photonic technologies appears.

The 120-GHz-band wireless link using InP HEMT MMICs has the merits of a small size, simple structure, light weight, low power consumption and low cost because all functions are implemented into millimeter-size MMIC chips. Therefore, it can be assembled quickly and is easy to operate. Moreover, it now consumes less than 100 W, so that it can be operated using a 12-V battery. On the other hand, it is impossible to change the modulation scheme and operation frequency. Due to these features, the 120-GHz-band wireless link using InP HEMT MMIC technologies is suitable for live TV relay because there is a strong demand to reduce the time required from arrival on the site to becoming broadcast-ready to broadcast much as possible. Wireless links for disaster recovery and temporary wireless links for public viewing and large-scale events are also promising applications of the 120-GHz-band wireless link using InP HEMT MMICs.

VII. Investigation of Transmission Distance

The attenuation of 120-GHz-band MMW signals by atmosphere and rain is large compared with microwave signals. Therefore, it is important to take these attenuations into consideration in estimating the transmission distance of 120-GHz-band wireless link. We have already reported measurement results of rain attenuation on a 120-GHz band wireless link from March to December, 2008 [30]. To increase the accuracy of the statistical analysis, we continued the measurement of rain attenuation using the same experimental setup to the end of September 2009, giving us a total measurement period of one year and seven months. The wireless link is set up at the NTT Atsugi R&D Center. The experimental site in Atsugi (Japan) is at latitude $35^\circ\ 26'$N and longitude $139^\circ\ 18'$E and about 93 m above sea level. The length of the link is about 400 m.

Fig. 23 shows the rain rate cumulative distribution from March 2008 to October 2009 in the Atsugi, Japan, area. In this work, the rain rate was calculated by multiplying the experimental results for the one-minute rain rate by 60 to express the rain rate in millimeters per hour and thereby make comparisons with other technical reports easy. The rain rate for 0.1%, 0.01% and 0.001% cumulative distributions are 25, 58 and 96 mm/hr, respectively. We compared the result with the theoretical cumulative distribution models, i.e., conditional M distribution [31], and the conditional M distribution agrees well over the region of 0.03%.

Fig. 24 shows the dependence of the attenuation coefficient due to rain on the one-minute rain rate during the same period as in Fig. 23. In general, the specific attenuation A (dB/km) is approximately expressed as

$$A = aR^b \tag{11}$$

where R is the rain rate (mm/hr) and a and b are functions of frequency, dropsize distribution and rain temperature [32]. In the ITU model, a is 1.13 and b is 0.732. The specific attenuation using the ITU model is also shown in Fig. 24. The measurement

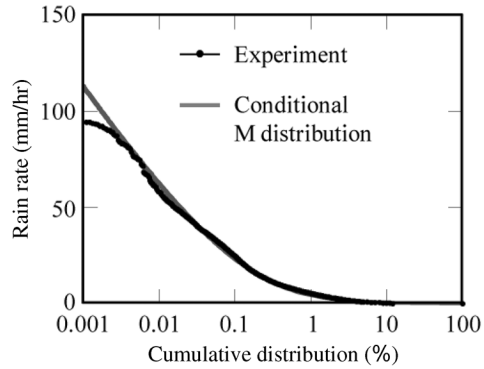

Fig. 23. Rain rate cumulative distribution from March 2008 to October 2009 in the Atsugi, Japan, area.

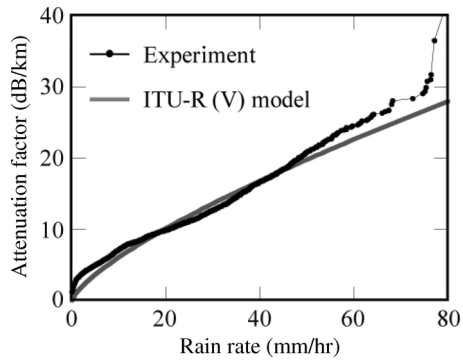

Fig. 24. Dependence of the attenuation coefficient due to rain on the one-minute rain rate from March 2008 to October 2009 in the Atsugi, Japan, area.

results agree well with the ITU model in the range from 10 to 80 mm/hr. The rain attenuation obtained by the year-round measurement is about 9, 17 and 23 dB/km when the rain rate is 20, 40 and 60 mm/hr, respectively.

Using these statistical analysis results, we investigated the dependence of transmission distance on the output power as a parameter of availability. The received power (P_r) is given by

$$P_r(\text{dB}) = Pt + Gt + Gr - 20 \times \log\left(\frac{4\pi d}{\lambda}\right) - (L_1 + A_1) \times d \tag{12}$$

where Pt is transmitter output power, d is transmission distance, λ is wavelength, Gt is transmitter antenna gain, Gr is receiver antenna gain, and L_1 is atmospheric gaseous loss, and A_1 is rain attenuation coefficient. We assumed the maximum transmission distance $(d_{\max})$ to be the distance where P_r calculated by (12) is below -44 dBm, which is the minimum received power necessary for a BER of 10^{-12}. We changed the value of A_1 depending the availability obtained by the cumulative distribution of the rain rate shown in Fig. 23.

The calculation results are shown in Fig. 25 for G_t and G_r of 52 dBi. In fine weather, $\mathrm{d}_{\max}$ is about 10 km when P_t is 16 dBm. When P_t increases to 20 and 30 dBm, $d_{\max}$ is about 13 and 20 km, respectively. On the other hand, $d_{\max}$ decreases drastically due to the rain attenuation. In order to guarantee the availability of 99.9% and 99.999% (rain rate: 25 and 96 mm/hr), $d_{\max}$ becomes about 1.8 and 1.0 km, respectively, when P_t is 16 dBm. The increase in P_t up to 30 dBm does not affect $d_{\max}$

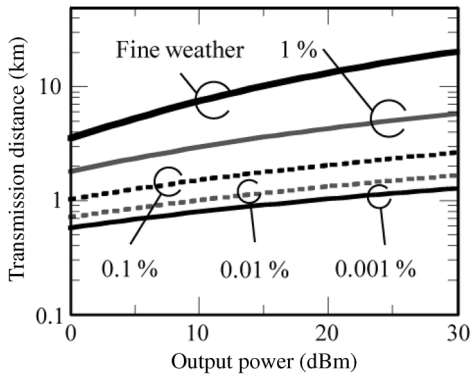

Fig. 25. Calculation results of relationship between the transmission distance and output power as a parameter of output power and availability. The antenna gain is 52 dBi.

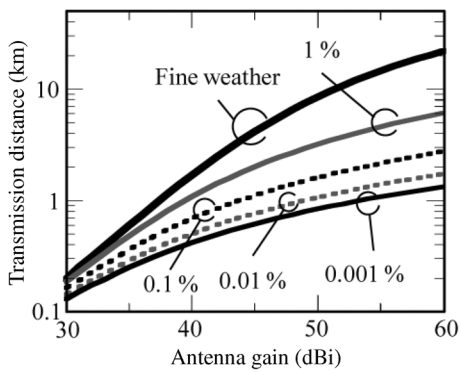

Fig. 26. Calculation results of transmission distance as a parameter of antenna gain and availability. The output power is 16 dBm.

in heavy rain condition so much compared with that in the fine weather conditions, and $d_{\max}$ becomes about 2.6 and 1.3 km for the 99.9% and 99.999% availability, respectively. As discussed in Section III, PAs based on InP HEMT MMICs have already achieved 16-dBm $P_{1\ \mathrm{dB}}$ output power and have a potential to generate 20-dBm $P_{1\ \mathrm{dB}}$ output power at 125 GHz. On the other hand, it is difficult to achieve 30-dBm $P_{1\ \mathrm{dB}}$ output power with state-of-the-art InP HEMT MMIC technology. Therefore, it may be possible to transmit 10-Gbit/s data over a distance of 10 km in a fine weather, however, it will be difficult to achieve a 20-km-long transmission distance in the near future.

Fig. 26 shows the dependence of $d_{\max}$ on antenna gain as a parameter of availability when P_t is 16 dBm. When antenna gain is 30 dBi, $d_{\max}$ is about 200 m in fine weather. For availability of 99.999%, $d_{\max}$ is about 130 m. When we use a 60-dBi antenna, $d_{\max}$ is over 20 km in fine weather. These results indicate that the 120-GHz-band wireless link has the potential to transmit 10-Gbit/s data over a distance of 10 km in a fine weather and that it guarantee the transmission distance of about 1 km with availability of 99.999% in Japan.

VIII. Conclusion

For outdoor applications of 120-GHz-band wireless links, increasing output power and receiver sensitivity is very important. The key devices for the generation of 120-GHz-band wireless signal are a UTC-PD and InP HEMT MMIC. The maximum output power of the UTC-PD mainly depends on the carrier transit time-limited bandwidth and PD junction area, and the state-of-the-art UTC-PD can generate about 8-dBm output power at 125 GHz by introducing a matching circuit. For the InP HEMT MMIC, breakdown voltage mainly determines the maximum output power, and we have achieved a $P_{1\ \mathrm{dB}}$ of 16 dBm by using composite channel InP HEMT MMICs with improved breakdown voltage. The phase noise of 125-GHz CW signals generated by UTC-PDs and InP HEMTs are almost the same, about -90 dBc/Hz at an offset frequency of 100 kHz. Due to the increase in the output power and receiver sensitivity of the 120-GHz-band wireless link, we have achieved a 10-Gbit/s data transmission over a distance of 5.8 km in a fine weather.

We investigated the transmission distance dependence of availability using statistical rain attenuation obtained at Atsugi Japan for over one year. The rain attenuation statistics data show that the 120-GHz-band wireless link can transmit 10-Gbit/s data over a distance of 1 km with availability of 99.999%.

Acknowledgment

The authors would like to thank Dr. T. Enoki for his encouragement and discussions.

References

[1] J. M. Gilbert, C. H. Doan, S. Emami, and C. B. Shung, "A 4-Gbps uncompressed wireless HD A/V transceiver chipset," *IEEE Micro*, vol. 28, pp. 56–64, 2008.

[2] A. Hirata, R. Yamaguchi, T. Kosugi, H. Takahashi, K. Murata, T. Nagatsuma, N. Kukutsu, Y. Kado, N. Iai, S. Okabe, S. Kimura, H. Ikegawa, H. Nishikawa, T. Nakayama, and T. Inada, "10-Gbit/s wireless link using InP HEMT MMICs for generating 120-GHz-band millimeter-wave signal," *IEEE Trans. Microw. Theory Tech.*, vol. 57, no. 5, pt. 1, pp. 1102–1109, May 2009.

[3] T. Ishibashi, T. Furuta, H. Fushimi, S. Kodama, H. Ito, T. Nagatsuma, N. Shimizu, and Y. Miyamoto, "InP/InGaAs uni-traveling-carrier photodiodes," *IEICE Trans. Electron.*, vol. E83-C, no. 6, pp. 938–949, 2000.

[4] T. Kosugi, T. Shibata, T. Enoki, M. Muraguchi, A. Hirata, T. Nagatsuma, and H. Kyuragi, "A 120-GHz millimeter-wave MMIC chipset for future broadband wireless application," in *IEEE MTT-S Int. Microw. Symp. Dig.*, 2003, vol. 1, pp. 129–132.

[5] A. Hirata, N. Sahri, H. Ishii, K. Machida, S. Yagi, and T. Nagatsuma, "Design and characterization of millimeter-wave antenna for integrated photonic transmitter," in *Proc. Asia–Pacific Microwa. Conf.*, Sydney, Australia, Dec. 3–6, 2000, pp. 70–73.

[6] A. Hirata, M. Harada, and T. Nagatsuma, "120-GHz wireless link using photonic techniques for generation, modulation, and emission of millimeter-wave signals," *J. Lightw. Technol.*, vol. 21, no. 10, pp. 2145–2153, Oct. 2003.

[7] T. Minotani, A. Hirata, and T. Nagatsuma, "A broadband 120-GHz Schottky-diode receiver for 10-Gbit/s wireless links," *IEICE Trans. Electron.*, vol. E86-C, no. 8, pp. 1501–1505, 2003.

[8] A. Hirata, T. Kosugi, T. Shibata, and T. Nagatsuma, "High-directivity photonic emitter using photodiode module integrated with HEMT amplifier for 10-Gbit/s wireless link," *IEEE Trans. Microw. Theory Tech.*, vol. 52, no. 8, pp. 1843–1850, Aug. 2004.

[9] A. Hirata, T. Kosugi, H. Takahashi, J. Takeuchi, K. Murata, N. Kukutsu, Y. Kado, S. Okabe, T. Ikeda, F. Suginosita, K. Shogen, H. Nishikawa, A. Irino, T. Nakayama, and N. Sudo, "5.8-km 10-Gbps data transmission over a 120-GHz-band wireless link," in *Proc. IEEE Int. Conf. Wireless Inf. Technol. Syst.*, 2010, paper 207.1.

[10] M. R. Kumar, D. Kumar, and A. K. Shukla, "Development of D-band Gunn oscillator," in *Proc. Int. Conf. Recent Adv. Microw. Theory Applic.*, 2008, pp. 316–318.

[11] J. Wenger and S. Huber, "Low-noise D-band IMPATT oscillators," *Electron. Lett.*, vol. 23, pp. 475–476, 1987.

[12] A. R. Harvey, G. M. Smith, and J. C. G. Lesurf, "Phase noise measurements of a D-band backward wave oscillator," *IEEE Microw. Guided Wave Lett.*, vol. 4, pp. 271–273, 1994.

[13] R. Lai, X. B. Mei, W. R. Deal, W. Yoshida, Y. M. Kim, P. H. Liu, J. Lee, J. Uyeda, V. Radisic, M. Lange, T. Gaier, L. Samoska, and A. Fung, "Sub 50 nm InP HEMT device with fmax greater than 1 THz," in *Proc. IEEE Int. Electron Devices Meeting*, 2007, pp. 609–611.

[14] T. Kosugi, H. Sugiyama, K. Murata, H. Takahashi, A. Hirata, N. Kukutsu, Y. Kado, and T. Enoki, "A 125-GHz 140-mW InGaAs/InP composite-channel HEMT MMIC power amplifier module," *IEICE Electron. Exp.*, vol. 6, pp. 1764–1768, 2009.

[15] H. Ito, T. Nagatsuma, A. Hirata, T. Minotani, A. Sasaki, Y. Hirota, and T. Ishibashi, "High-power photonic millimetre wave generation at 100 GHz using matching-circuit-integrated uni-travelling-carrier photodiodes," *Proc. Inst. Electr. Eng.—Optoelectron.*, vol. 150, no. 2, pp. 138–142, 2003.

[16] H. Sugiyama, T. Kosugi, H. Yokoyama, K. Murata, Y. Yamane, M. Tokumitsu, and T. Enoki, "High-performance InGaAs/InP composite-channel high electron mobility transistors grown by metal-organic vapor-phase epitaxy," *Jpn. J. Appl. Phys.*, vol. 47, no. 4, pp. 2828–2832, 2008.

[17] T. Kosugi, M. Tokumitsu, K. Murata, T. Enoki, H. Takahashi, A. Hirata, and T. Nagatsuma, "120-GHz Tx/Rx waveguide modules for 10-Gbit/s wireless link system," in *IEEE Compound Semicond. IC Symp. Dig.*, Nov. 2006, pp. 25–28.

[18] M. Micovic, A. Kurdoghlian, K. Shinohara, S. Burnham, I. Milosavljevic, M. Hu, A. Corrion, A. Fung, and R. Lin, "W-band GaN MMIC with 842 mW output power at 88 GHz," in *IEEE MTT-S Int. Microw. Symp. Dig.*, 2010, pp. 237–239.

[19] W. R. Deal, X. B. Mei, V. Radisic, B. Bayuk, A. Fung, W. Yoshida, P. H. Liu, J. Uyeda, L. Samoska, T. Gaier, and R. Lai, "A new sub-millimeter wave power amplifier topology using large transistors," *IEEE Microw. Wireless Compon. Lett.*, vol. 18, no. 8, pp. 542–544, 2008.

[20] S. Sekino, *Basis of Digital Modulation and Demodulation Circuit* (in Japanese). Tokyo, Japan: Ohm, pp. 30–35.

[21] H. Takahashi, T. Kosugi, A. Hirata, K. Murata, and N. Kukutsu, "120-GHz-band low-noise amplifier with 14-ps group-delay variation for 10-Gbit/s data transmission," in *Proc. 38th Eur. Microw. Conf.*, Amsterdam, The Netherlands, Oct. 27–31, 2008, pp. 1457–1460.

[22] A. Hirata, N. Iai, R. Yamaguchi, H. Takahashi, T. Kosugi, K. Murata, N. Kukutsu, Y. Kado, S. Kimura, S. Okabe, H. Ikegawa, H. Nishikawa, T. Nakayama, and T. Inada, "10-Gbit/s data transmission with forward error correction using a 120-GHz-band wireless link," presented at the Asia–Pacific Microw. Conf., Macau, China, Dec. 16–20, 2008, A3-11.

[23] H. Takahashi, T. Kosugi, A. Hirata, K. Murata, and N. Kukutsu, "10-Gbit/s BPSK modulator and demodulator for a 120-GHz-band wireless link," *IEEE Trans. Microw. Theory Tech.*, vol. 59, no. 5, pp. 1361–1368, May 2011.

[24] A. Hirata, H. Ishii, and T. Nagatsuma, "Design and characterization of a 120-GHz millimeter-wave antenna for integrated photonic transmitters," *IEEE Trans. Microw. Theory Tech.*, vol. 49, no. 11, pp. 2157–2162, Nov. 2001.

[25] A. Hirata, T. Furuta, and T. Nagatsuma, "Monolithically integrated Yagi-Uda antenna for photonic emitter operating at 120 GHz," *Electron. Lett.*, vol. 37, no. 18, pp. 1107–1109, Aug. 2001.

[26] A. Hirata, T. Minotani, and T. Nagatsuma, "A 120-GHz microstrip antenna monolithically integrated with a photodiode on Si," *Jpn. J. Appl. Phys.*, vol. 41, no. 3A, pt. 1, pp. 1390–1394, Mar. 2002.

[27] A. Hirata, H. Togo, N. Shimizu, H. Takahashi, K. Okamoto, and T. Nagatsuma, "Low-phase noise photonic millimeter-wave generator using an AWG integrated with a 3-dB combiner," *IEICE Trans. Electron.*, vol. E88-C, no. 7, pp. 1458–1464, Jul. 2005.

[28] H. Ito, T. Furuta, A. Hirata, T. Kosugi, Y. Muramoto, M. Tokumitsu, T. Nagatsuma, and T. Ishibashi, "Pre-amplifier-integrated uni-traveling-carrier photodiode module with a rectangular waveguide-output port for operation in the 120-GHz band," in *Proc. IEEE LEOS Conf.*, 2004, vol. 1, pp. 128–129.

[29] R. T. Logan, Jr., "All-optical heterodyne RF signal generation using a mode-locked-laser frequency comb: Theory and experiments," in *IEEE MTT-S Int. Microw. Symp. Dig.*, 2000, vol. 3, pp. 1741–1744.

[30] A. Hirata, R. Yamaguchi, H. Takahashi, T. Kosugi, K. Murata, N. Kukutsu, and Y. Kado, "Effect of rain attenuation for a 10-Gb/s 120-GHz-band millimeter-wave wireless link," *IEEE Trans. Microw. Theory Tech.*, vol. 57, no. 12, pt. 2, pp. 3099–3105, Dec. 2009.

[31] T. Taga, M. Ishida, and O. Sasaki, "Comparison of methods for estimating one-minute rainfall rate distribution and proposal of a method using conditional M distribution" (in Japanese) Tech. Rep. IEICE, AP2007-57, 2002, pp. 7–12.

[32] "Propagation data and prediction methods required for the design of terrestrial line-of-sight systems," ITU, Geneva, Switzerland, Rec. ITU-R P.530-11, Sep. 2006.

Akihiko Hirata (SM'11) received the B.S. and M.S. degrees in chemistry and Dr. Eng. degree in electrical and electronics engineering from Tokyo University, Tokyo, Japan, in 1992, 1994, and 2007, respectively.

He joined Nippon Telegraph and Telephone Corporation (NTT), Atsugi Electrical Communications Laboratories (presently NTT Microsystem Integration Laboratories), Kanagawa, Japan, in 1994. He is currently a Senior Research Engineer and Supervisor with NTT Microsystem Integration Laboratories. His current research involves millimeter-wave antenna and ultra-broadband millimeter-wave wireless system.

Dr. Hirata is a member of the Institute of Electrical, Information and Communication Engineers (IEICE) of Japan. He received the 2002 Asia–Pacific Microwave Conference APMC prize, the 2004 YRP Award, the 2007 Achievement Award presented by the IEICE, the 2008 Maejima Award presented by the Post and Telecom Association of Japan, 2009 Radio Achievement Award presented by Association of Radio Industries and Businesses Broadcast-Culture, 2010 Fundation Award presented by Hoso Bunka Fundation, 2010 Asia–Pacific Microwave Conference APMC prize, and the 2011 Commendation for Science and Technology by the Minister of Education, Culture, Sports, Science and Technology.

Toshihiko Kosugi received the M.S. and Ph.D. degrees in electrical engineering from Osaka University, Osaka, Japan, in 1990 and 1993, respectively. His Ph.D. dissertation addressed the characterization of point defects in GaAs and processing of GaAs.

In 1993, he joined Nippon Telegraph and Telephone Corporation (NTT). He is currently with NTT Photonics Laboratories, Kanagawa, Japan, studying the microwave characteristics of HEMTs on InP and their application in MMICs.

Dr. Kosugi received the 2007 Achievement Award presented by the Institute of Electronics, Information, Communication Engineers (IEICE), the 2008 Maejima Award presented by the Post and Telecom Association of Japan, and the 2011 Commendation for Science and Technology by the Minister of Education, Culture, Sports, Science and Technology.

Hiroyuki Takahashi (M'11) received the B.S. and M.S. degrees in applied physics from Nagoya University, Nagoya, Japan, in 2001 and 2003, respectively.

In 2003, he joined Nippon Telegraph and Telephone (NTT) Microsystem Integration Laboratories, NTT Corporation, Atsugi-shi, Japan. He is engaged in research and development of millimeter-wave MMICs. His other research interests include ultra-high-speed wireless technologies.

Mr. Takahashi is a member of the Institute of Electrical, Information and Communication Engineers (IEICE) of Japan. He received the 2008 Young Engineers Prize presented by the European Microwave Integrated Circuits Conference.

Jun Takeuchi received the B.E. and M.E. degrees from Tokyo Institute of Technology, Tokyo, Japan, in 2006 and 2008, respectively.

In 2008, he joined Nippon Telegraph and Telephone (NTT) Microsystem Integration Laboratories, NTT Corporation, Atsugi-shi, Japan. He is engaged in research and development of millimeter-wave components and wireless systems.

Mr. Takeuchi is a member of he Institute of Electrical, Information and Communication Engineers (IEICE) of Japan. He received the 2010 Asia–Pacific Microwave Conference APMC prize.

Hiroyoshi Togo (SM'11) received the M.Sc. and Ph.D. degrees in applied physics and electronic engineering from University of Tsukuba, Ibaraki, Japan, in 1996 and 2010, respectively.

He joined the Nippon Telegraph and Telephone Corporation (NTT), Musashino Opto-electronics Laboratories in 1996. From 1996 to 2001, he was engaged in the development of the thermo-capillary waveguide-based optical switch and from 2001 to 2002 he endeavored to commercialize it for NTT Electronics Inc. Since 2002, he has been researching ultrawideband impulse radio systems using photonic techniques and millimeter-wave tomography with electro-optic probing, and is now a senior research engineer at NTT Microsystem Integration Laboratories, Kanagawa, Japan.

Dr. Togo is a member of the IEEE Photonics Society, the IEEE Antenna and Propagation Society, the IEEE Microwave Theory and Techniques Society (MTT-S), and the Institute of Electronics, Information and Communication Engineers of Japan. He was a recipient of the 2006 Asia–Pacific Microwave Photonics Conference AP-MWP Award and the 2010 European Conference on Antenna and Propagation Award.

Makoto Yaita received the B.S. and M.E. degrees from Waseda University, Tokyo, Japan, in 1988 and 1990, respectively.

In 1990, he joined Nippon Telegraph and Telephone Corporation (NTT), LSI Laboratories, Kanagawa, Japan, where he was engaged in the research and development of measurement technologies for high-speed devices and ultrafast-optical signals. From 1999 to 2008, he had been engaged in the development of the digital television relay network in NTT Communications. He is currently a Senior Research Engineer and Supervisor with NTT Microsystem Integration Laboratories. His current research involves millimeter-wave radio transmission.

Mr. Yaita is a member of the Institute of Electronics, Information and Communication Engineers of Japan.

Naoya Kukutsu (M'93) was born in Hokkaido, Japan, on September 16, 1962. He received B.E., M.E., and D.E. degrees in electrical engineering from Hokkaido University, Sapporo, Japan, in 1986, 1988, and 1991, respectively. His D.E. dissertation described research on a time-domain electromagnetic wave numerical analysis method.

In 1991, he joined Nippon Telegraph and Telephone Corporation (NTT), Applied Electronics Laboratories, Musashino, Japan. He is currently a senior research engineer and supervisor at NTT Microsystem Integration Laboratories, Atsugi, Japan. His current research involves millimeter-wave radio transmission and millimeter-wave imaging systems.

Dr. Kukutsu is a member of the IEEE Micowave Theory and Techniques Society (MTT-s), the IEEE Communications Society, and the Institute of Electronics, Information and Communication Engineers of Japan.

Kimihisa Aihara (M'09) received B.E. degrees in electronics from Keio University, Tokyo, Japan, in 1984.

In 1984, he joined Nippon Telegraph and Telephone Public Corporation (now NTT). He is currently responsible for ubiquitous communications appliance technologies at NTT Microsystem Integration Laboratories as an executive manager. He is leading R&D projects on subterahertz-wave wireless communications, ultra-low-power network appliances and electric near-field communication for human area network.

Koichi Murata (SM'92) received the B.S. and M.S. degrees in mechanical engineering and Dr. Eng. degree in electrical and electronics engineering from Nagoya University, Nagoya, Japan, in 1987, 1989, and 2003, respectively.

He joined NTT LSI Laboratories, Atsugi, Japan, in 1989. He is currently a Senior Research Engineer and Supervisor at NTT Photonics Laboratories, Atsugi, Japan. He has been engaged in research and development of ultrahigh-speed mixed-signal ICs for optical communications systems. His current research interests include optoelectronic IC design and high-speed optical transmission systems.

Dr. Murata is a member of the Institute of Electronics, Information and Communication Engineers of Japan.

Yasuhiro Sato (M'97) received the B.S., M.S., and Ph.D. degrees in chemistry from the University of Tokyo, Tokyo, Japan, in 1987, 1989 and 2004, respectively.

In 1989, he joined NTT LSI Laboratories, Atsugi, Japan. From 1989 to 2004, he worked on LSI interconnection technology, ultra-thin-film CMOS/SOI process integration for low power application, and low-power communication appliances for ubiquitous services. He is currently engaged in research and development of millimeter-wave wireless communication technology.

Dr. Sato is a member of the Japan Society of Applied Physics, and the Institute of Electronics, Information and Communication Engineers of Japan.

Tadao Nagatsuma (M'93–SM'02) received the B.S., M.S., and Ph.D. degrees in electronic engineering from Kyushu University, Fukuoka, Japan, in 1981, 1983, and 1986, respectively. During his Ph.D. studies, he was involved in millimeter-wave and submillimeter-wave oscillators based on flux-flow phenomenon in superconducting devices. In 1986, he joined the Electrical Communications Laboratories, Nippon Telegraph and Telephone Corporation (NTT), Atsugi, Kanagawa, Japan, where he was engaged in research on the design and testing of ultrahigh-speed semiconductor electronic/photonic devices and integrated circuits. From 1999 to 2002, he was a Distinguished Technical Member with NTT Telecommunications Energy Laboratories. From 2003 to 2007, he was a Group Leader with NTT Microsystem Integration Laboratories. He is currently a Professor at the Division of Advanced Electronics and Optical Science, Department of Systems Innovation, Graduate School of Engineering Science, Osaka University, Toyonaka, Japan. His research interests include millimeter-wave and terahertz photonics and their application to sensors and wireless communications.

Prof. Nagatsuma is a member of the Institute of Electronics, Information and Communication Engineers (IEICE), Japan, the Technical Committee on Microwave Photonics of the IEEE Microwave Theory and Techniques Society, and the Microwave Photonics Steering Committee. He was the recipient of the 1989 Young Engineers Award presented by the IEICE, the 1992 IEEE Andrew R. Chi Best Paper Award, the 1997 Okochi Memorial Award, the 1998 Japan Microwave Prize, the 2000 Minister's Award of the Science and Technology Agency, the 2002 Asia–Pacific Microwave Conference Prize, the 2004 Yokosuka Research Park Award, the 2006 Asia–Pacific Microwave-Photonics Conference Award, the 2006 European Microwave Conference Prize, the 2007 Achievement Award presented by the IEICE, the 2008 Maejima Award presented by the Post and Telecom Association of Japan, the 2009 Education and Research Award from Osaka University, the 2011 Commendation for Science and Technology by the Minister of Education, Culture, Sports, Science and Technology, and the 2011 Recognition from Kinki Bureau of Telecommunications, Ministry of Internal Affairs and Communications.

Yuichi Kado (M'08) received the M.S. and Ph.D. degrees in electronics from Tohoku University, Miyagi, Japan, in 1983 and 1998, respectively.

In 1983, he joined the Electrical Communication Laboratories of Nippon Telegraph and Telephone Public Corporation (now NTT), Kanagawa, Japan, where he was engaged in research on SOI structure formation by hetero-epitaxial growth. From 1989 to 1998 he worked on the development of fully depleted CMOS/SIMOX LSIs and ultra-low-power CMOS circuits. From 1999, he was engaged in R&D on compact network appliances using ultralow-power CMOS circuit technologies for ubiquitous communications. He led research and development projects on ultra-low-power network appliances, sub-terahertz-wave wireless communication, and intra-body communication as a Director of Smart Devices Laboratory at NTT Microsystem Integration Laboratories (2003–2010). In July 2010, he joined the Department of Electronics, Kyoto Institute of Technology, Kyoto, Japan.

Dr. Kado was the recipient of awards including the 1990 Young Engineers Award presented by the Institute of Electronics, Information and Communication Engineers of Japan, the 2009 Nikkei BP Technology Award, and the 2009 Radiowave Achievement Award presented by the ARIB.